ACS PHYSICAL CHEMISTRY Au
AN OPEN ACCESS JOURNAL OF THE AMERICAN CHEMICAL SOCIETY

pubs.acs.org/physchemau

Article

Fano-Type Wavelength-Dependent Asymmetric Raman Line Shapes from MoS_2 Nanoflakes

Manushree Tanwar, Love Bansal, Chanchal Rani, Sonam Rani, Suchita Kandpal, Tanushree Ghosh, Devesh K. Pathak, I. Sameera, Ravi Bhatia, and Rajesh Kumar*

Cite This: *ACS Phys. Chem Au* 2022, 2, 417–422

Read Online

ACCESS | Metrics & More | Article Recommendations

ABSTRACT: Excitation wavelength-dependent Raman spectroscopy has been carried out to study electron–phonon interaction (Fano resonance) in multi-layered bulk 2H–MoS_2 nano-flakes. The electron–phonon coupling is proposed to be caused due to interaction between energy of an excitonic quasi-electronic continuum and the discrete one phonon, first-order Raman modes of MoS_2. It is proposed that an asymmetrically broadened Raman line shape obtained by 633 nm laser excitation is due to electron–phonon interaction whose electronic continuum is provided by the well-known A and B excitons. Typical wavelength-dependent Raman line shape has been observed, which validates and quantifies the Fano interaction present in the samples. The experimentally obtained Raman scattering data show very good agreement with the theoretical Fano–Raman line-shape functions and help in estimating the coupling strength. Values of the electron–phonon interaction parameter obtained, through line-shape fitting, for the two excitation wavelengths have been compared and shown to have generic Fano-type dependence on the excitation wavelength.

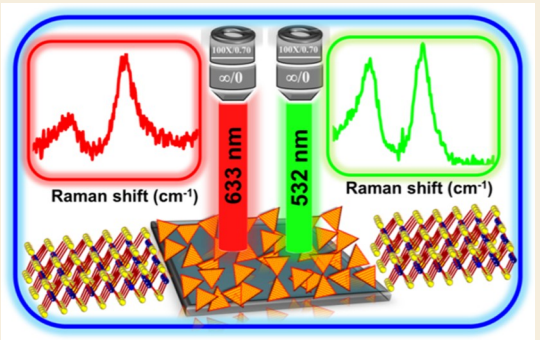

KEYWORDS: *electron–phonon interaction, Fano resonance, Raman line shape, MoS_2, light–matter interaction, 2-D materials*

INTRODUCTION

Light–matter interaction in transition metal chalcogenides[1] like MoS_2, $MoSe_2$,WS_2, and WSe_2 has been widely explored to make next-generation photonics and optical devices[1] by exploring their unique electronic,[2−4] optical,[5] and spin-valleytronic[6] and electrical[7] properties. Among these, MoS_2 has gained tremendous attention due to its application in light detection,[8] light emission,[9] solar energy storage,[10] field-effect transistors (FETs),[11,12] and so forth. To be used in device applications, the material should be well versed with its optical, vibronic, and electronic properties and their interplay, if any, present, in the material of interest. For example, electron–phonon interaction[13] commonly known as Fano resonance, which is a prominent phenomenon affecting lattice thermal conductivity[14] and carrier transport[15] and governing optical properties of the material, needs to be carefully analyzed in any material prior to its use in devices. U. Fano, for the first time, gave the theoretical explanation of asymmetric line shape based on the superposition principle of quantum mechanics. The effect of Fano resonance is observed in various systems where there is a strong interaction of a discrete state and a degenerate continuum, with its first observation in the atomic system.[16] Since its first report in 1961, a variety of systems have been found to exhibit Fano resonance that manifests in different genres like non-linear Fano resonance,[17] Fano scattering,[18] and so forth, making it a topic worth exploring in different materials including in their nano-regimes. For example, in a two-oscillator system with a driving force when the frequency of the latter is equal to the eigenfrequency of the oscillator, the amplitude of the oscillator grows toward the maximum value. In a weakly coupled oscillator system, there are two resonance frequencies in which the first resonance is characterized using Breit–Wigner resonance, whereas the second frequency is characterized using an asymmetric profile. Fano resonance manifests itself in terms of asymmetric line-shape profiles comprising a dip called the anti-resonance dip or minima and a peak corresponding to the maxima of resonance.

Raman spectroscopy[19−24] is a widely used non-destructive tool to study Fano resonance and hence can be employed to study the perturbed electronic–vibronic properties and their interplay in transition metal dichalcogenides. In bulk materials, Fano resonance takes place due to matching of energy of the electronic continuum provided by free carriers via either heavy

Received: April 1, 2022
Revised: May 6, 2022
Accepted: May 6, 2022
Published: May 20, 2022

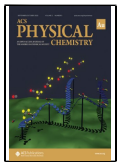

https://doi.org/10.1021/acsphyschemau.2c00021
ACS Phys. Chem Au 2022, 2, 417–422

doping[25,26] or photoexcited carriers,[27,28] with the discrete one-phonon energy, causing a constructive and destructive interference.[16,29] Such a perturbation is manifested in terms of asymmetric Raman line-shape profiles and is often shifted in terms of its peak position. Another prominent feature of these Raman profiles depicting Fano resonance is the presence of antiresonance (dip) on either the pre-maximum or post-maximum side[30] depending on the type of carrier (electron or hole) involved in generating the electronic continuum. To analyze the effect of resonance, parametric Raman line shape analysis is done. The Raman line shape parameters[31] to assess the perturbation in line shape include the peak position, full width at half-maximum (fwhm),[32] and asymmetry ratio (α_R) defined by the ratio of lower half width (Γ_L) to higher half width (Γ_H), that is, $\alpha_R = \Gamma_L/\Gamma_H$ of the observed Raman spectrum.

Raman vibrational modes of 2H−MoS_2 include four first-order Raman active modes, namely, E^2_{2g}, E_{1g}, E^1_{2g}, and A_{1g} with the Raman line shape centered at approximately 32, 286, 378, and 408 cm^{-1}, respectively, for the bulk phase. The E^2_{2g} mode involves the interlayer mode caused by the vibration of two rigid layers against each other, and the E_{1g} mode is forbidden in backscattering geometry on the surface perpendicular to the *c* axis. All the modes, except E^2_{2g}, involve the intra-layer (S−Mo−S) atomic vibrations.[33] The characteristic modes, namely, E^1_{2g} and A_{1g} have been widely explored due to shift in only the peak position of the symmetric Raman line shape obtained by changing layer thickness.[34] The energies of these discrete modes are in the range of a few tens of millielectron volt which may participate in Fano-type interaction if a system possesses an appropriate continuum. Bulk MoS_2 is known to have two excitonic energy states corresponding to A and B excitons,[3,35,36] separated by a couple of hundred millielectron volt, which may provide the necessary quasi-continuum of states which can enable the Fano coupling with the discrete phonons. Since there is no fundamental restriction which can prohibit the Fano resonance from taking place, it would be interesting to study MoS_2-type two-dimensional (2D) systems to explore the presence of Fano interaction using Raman spectroscopy.

The current paper deals with the parametric spectral line shape analysis of the observed asymmetric Raman spectrum obtained from multi-layered MoS_2 nanoflakes (MLMNs). The presence of asymmetry in the Raman line shape hints at the presence of electron−phonon interaction which, in this case, is caused by energy resonance between an exciton-mediated electronic continuum of ∼100 meV and discrete one-phonon vibration modes, namely, E^1_{2g} and A_{1g}. The presence of the excitonic continuum is revealed by a broad photoluminescence (PL) emission. The origin of the electronic continuum has been identified as the energy difference between A and B exciton levels with the indirect band gap of 2H−MoS_2, which leads to the exciton-mediated Fano-like interference in bulk MoS_2. The presence of Fano resonance has been substantiated by strong wavelength-dependent Raman line-shape parameters. This has been further validated by theoretical line-shape fitting of the observed Raman scattering data using the Fano−Raman line-shape function which not only shows a good fit between the experiment and theoretical line shape but also helps in quantifying the Fano coupling strength. The variation in the wavelength-dependent Raman line-shape parameters, obtained from the line-shape fitting, shows the typical trend observed for systems where Fano-type resonance is present.

EXPERIMENTAL DETAILS

The MoS_2 nanoflakes have been synthesized by a facile one-step hydrothermal route.[37−40] In a typical synthesis, 1.7 g of ammonium heptamolybdatetetrahydrate [(NH4)6Mo7O24·4H2O] and 3 g of thiourea (CH_4N_2S) were dissolved in 60 ml of deionized water by continuous stirring for 30 min. Homogeneous and colorless solution was obtained, which was transferred into a 100 mL Teflon-lined stainless-steel autoclave. The autoclave was heated to 220 °C in an oven for a period of 24 h and then cooled down to room temperature. The MoS_2nano-flake sample, in the form of a black-colored product, was collected after centrifugation and was washed with deionized water and ethanol several times. At the end, the reaction product was dried using a freeze dryer at −80 °C in vacuum. A NOVA NanoSEM 450 field emission scanning electron microscopy (SEM) instrument and X-ray diffraction (XRD) instrument equipped with Cu K_α (Rigaku Miniflex-II) were employed for structural characterization of MoS_2. Raman spectroscopy measurements were carried out using a HORIBA-JobinYovn LABRAM HR spectrometer using 632 and 532 nm excitation using minimum laser power (1 mW).

RESULTS AND DISCUSSION

Structural characterization of the prepared MoS_2 sample has been carried out using SEM and XRD, whereas information about electronic states has been obtained using the photoluminescence (PL) technique. The hydrothermally prepared MoS_2 sample shows a nano-flake-like morphology as can be seen in the SEM images (Figure 1a). A zoomed view at higher

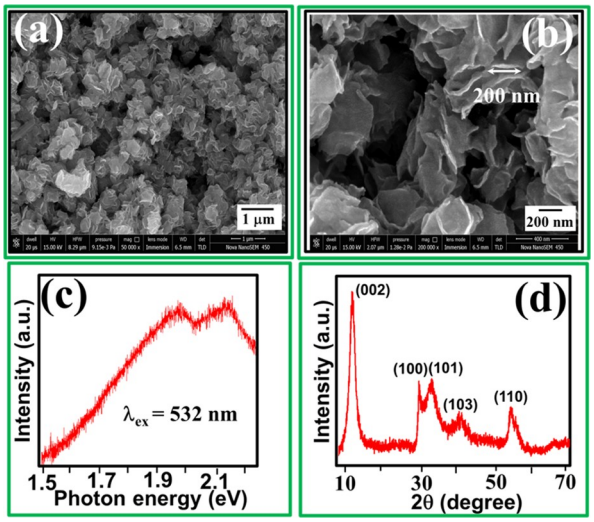

Figure 1. (a) SEM micrographs of MoS_2 nano-flakes and (b) magnified view showing the nano-petal-type morphology, (c) room-temperature PL spectrum recorded using 532 nm laser excitation, and (d) XRD pattern of MoS_2 nano-flakes. Reprinted in part with permission from *Solar Energy Materials and Solar Cells* **2021**, *236*, 111502.[2] Copyright 2022 Elsevier.

magnification (Figure 1b) confirms the formation of flower petal-shaped MLMNs with a petal thickness > 25 nm[41] representing multi-layered (bulk) MLMNs. Figure 1c shows the PL spectrum recorded using 532 nm excitation laser, showing the characteristic A and B excitons at 1.9 and 2.1 eV, respectively.[15,36] This further indicates the presence of MLMNs in the sample with ∼350 meV broad electronic states. The phase purity and crystallinity of these MLMNs have been confirmed by analyzing the XRD pattern of MLMNs (Figure 1d). The XRD pattern shows diffraction peaks of 2θ values of 14.06, 31.98, 35.36, 43.52, and 57.1° corresponding

https://doi.org/10.1021/acsphyschemau.2c00021
ACS Phys. Chem Au 2022, 2, 417−422

to (002), (100), (101), (103), and (110) planes, respectively, of MoS_2 which is in complete agreement with the standard card (JCPDS file no. 37-1492) confirming the 2H−MoS_2 phase. The sharp XRD peaks mean the presence of the crystalline structural phase.

To understand the vibrational properties of MoS_2, Raman spectroscopy has been employed. As discussed above, Raman line shape parameters deliver a wealth of information about the effect of perturbations on physical processes.[22,29,42−45] A typical Raman spectrum of Bulk MoS_2 consists of two characteristic modes, namely, E^1_{2g} and A_{1g}, arising due to in-plane and out-of-plane vibration modes,[34] wherein the in-plane mode consists of vibration of two S atoms in one direction and a Mo atom in the opposite direction. On the other hand, the out-of-plane mode consists of two S atoms vibrating opposite each other with a stationary Mo atom in between.[46] A symmetric Raman spectral line shape can easily represent these Raman modes, and no exception has been reported so far regarding the symmetric nature of the Raman spectrum. It is important here to mention that the Raman line shape, and associated symmetry, is sensitive to any perturbation in the system.[47,48] To dig out any possible interaction present at the microscopic level, Raman spectra have been recorded using 633 nm, and Raman line shape parameters have been extracted. Figure 2 shows the spectrum (red curve), recorded

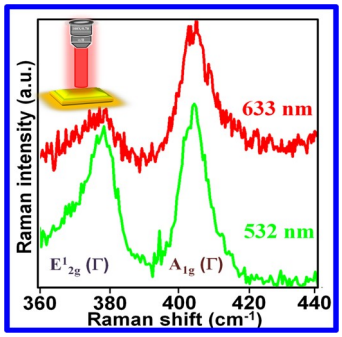

Figure 2. Experimentally obtained Raman spectra of MoS_2 flakes recorded using 633 and 532 nm laser excitation represented by red and green colors, respectively. The spectra have been recorded in backscattering geometry (inset).

using 633 nm excitation, with E^1_{2g} (378 cm^{-1}) and A_{1g} (404 cm^{-1}) modes having an asymmetry ratio (αR) of 1.4 and 0.7, respectively, estimated using the formula defined above. Raman line shape from bulk MoS_2[49] is symmetric with the two peaks observed around ∼377 and ∼405 cm^{-1}. In other words, the Raman modes (Figure 2) confirm that the sample is multi-layered and thus represented by bulk nature. Moreover, the separation between the E^1_{2g} and A_{1g} modes is more than 24 cm^{-1} which is another observation[41,50,51] that helps in ascertaining that the Raman spectroscopy sees these MLMNs as if they are in bulk regimes. Since the MLMNs are not limited by the number of layers, the presence of the quantum confinement effect, one of the typical reasons for an asymmetric Raman line shape, can be discounted in the MLMNs samples.

Presence of electron−phonon interaction (Fano effect) is another perturbation that is known to induce asymmetry in an otherwise symmetric Raman line shape.[16−18,52,53] As mentioned above, quantum confinement, which might have caused the asymmetry, is absent; Fano interaction could be a likely reason for the Raman line-shape asymmetry as seen in Figure 2. The presence of electron−phonon interaction, if any, also demands the presence of wavelength-dependent change in Raman line-shape parameters to confirm its presence. In an attempt to confirm this, the Raman spectrum from MLMNs has also been recorded from 532 nm excitation (in addition to 633 nm) as shown in Figure 2 (green curve). The E^1_{2g} and A_{1g} modes recorded with a 532 nm laser also represent asymmetric Raman line shape with α_R calculated as 1.2 and 0.8, respectively, which are different from the values obtained for the 633 nm spectrum (red curve, Figure 2). This is an additional observation which suggests the possible Fano interaction in addition to the observed inflated FWHM of 10 and 7 cm^{-1} for E^1_{2g} and A_{1g} modes, respectively. A report by Lee[54] et al. shows FWHM values for E^1_{2g} modes as ∼2 cm^{-1} (independent of layer thickness) and A_{1g} mode as ∼2.5 cm^{-1} for bulk MoS_2 where no Fano interaction is present. In other words, the wavelength-dependent variation in Raman line-shape parameters and inflated Raman line width are a strong indication of the presence of Fano interaction in the MLMNs which has manifested in terms of asymmetry in the Raman line shape (Figure 2). The same has been substantiated by theoretical fitting of the Raman data as discussed below. The theoretical explanation of the wavelength dependence of electron−phonon interaction is explained on the basis of the square of the electron−phonon interaction parameter (q), which represents the ratio of the scattering probability of the discrete state to that of the continuum, that is, $q \propto |R_p/R_e|$, where R_p and R_e are the Raman tensor for one-phonon and electronic Raman scattering[55] and are given by eqs 1 and 2, respectively.

$$R_p \propto \sum_i \frac{\langle 0|P_x|i\rangle\langle i|P_x|0\rangle}{[(\omega_f - \omega_i) - \omega_L]^2} \quad (1)$$

$$R_e \propto \sum_i \frac{\langle f|P_y|i\rangle\langle i|P_x|0\rangle}{[(\omega_f - \omega_i) - \omega_L]} \quad (2)$$

where $|0\rangle$ &$|f\rangle$ represent initial and final states, respectively; ω_L is the frequency of scattering radiation, and p is the linear momentum. Therefore, the relation of q with R_p and R_e shows the wavelength dependence of electron−phonon interaction.

As mentioned above, the electron−phonon interaction arises due to appropriate matching of energies of the electronic continuum arising by heavy doping,[55,56] by photo excitation of carriers,[27,28] and so forth, with the discrete one-phonon energy. The resonance of two energies leads to constructive or destructive interference, and the resulting perturbed line shape is characterized by Raman spectral parameters like ωo, FWHM, and αR. In this case, the possible quasi-electronic continuum is provided by exciton energies, and the same can be understood as follows. The room-temperature PL spectrum of MoS_2 nano-flakes (Figure 1c) shows two peaks at ∼1.9 and ∼2.2 eV corresponding to A and B excitons, respectively, arising due to transitions at the K point of the Brillouin zone.[15,57] It means that the discrete phonon modes can interact with this excitonic quasi-electronic continuum that can manifest itself as asymmetric Raman line shape as observed in Figure 2.

To further validate the presence and quantify the extent of electron−phonon interaction strength, theoretical fitting of experimentally obtained Raman spectra corresponding to E^1_{2g}

https://doi.org/10.1021/acsphyschemau.2c00021
ACS Phys. Chem Au 2022, 2, 417−422

and A_{1g} has been done using the Fano−Raman line-shape function[52,58] (eq 3) mentioned below

$$I(\omega) = \frac{(\epsilon + q)^2}{1 + \epsilon^2} \tag{3}$$

where $\varepsilon = \{(\omega - \omega_o)/(\Gamma/2)\}$, ω_o and Γ denote the phonon frequency and line width, respectively, and q is the Fano parameter and is the inverse of strength of electron−phonon coupling in any given system. Figure 3a,b shows experimentally

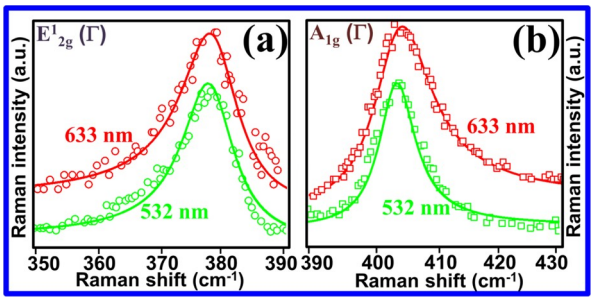

Figure 3. Theoretical fitting (solid lines) of experimentally observed Raman spectra (discrete points) of MoS_2 nano-flakes corresponding to E^1_{2g} mode (a) and A_{1g} mode (b) recorded using 633 and 532 nm laser excitation represented in red and green colors, respectively.

obtained Raman spectra (discrete data points) for E^1_{2g} and A_{1g} modes of MoS_2, respectively, fitted with the theoretical Fano−Raman line shape function (solid lines) represented by eq 3, for the two excitation wavelengths, namely, 633 and 532 nm. Figure 3 shows a good fit between the experimental Raman data and theoretical line-shape function (Fano−Raman equation) meaning a corroboration between the experimental data and the hypothesized Fano interaction. The values of q obtained, corresponding to the best fit, for both the E^1_{2g} and A_{1g} modes for 633 and 532 nm laser have been listed in Table 1. The trend of q versus λ_{exc} shows the typical Fano-type

Table 1. Estimated Fano Parameters (q) for E^1_{2g} and A_{1g} Modes for Different Excitation Wavelengths Obtained from Theoretical Fitting (Using eq 3) of Different Raman Spectra in Figure 3

excitation wavelength (nm)	q for E^1_{2g} mode	q for A_{1g} mode
633	−7 ± 0.35	7 ± 0.35
532	−12 ± 0.5	12 ± 0.5

wavelength dependence as shown in systems containing Fano interference[55,59] and is governed by eq 4

$$q \propto \frac{1}{\lambda_o - \lambda_{exc}} \tag{4}$$

where λ_o is the critical point energy corresponding to the electronic excitation at $k = 0$ in the band structure of MoS_2 and λ_{exc} is the energy of laser excitation. The value of λ_0 has been estimated by analyzing the wavelength-dependent trend (by extrapolating the trend) which comes out to be ∼2.91 eV.

The dependence of the electron−phonon coupling parameter on the excitation wavelength arises from the fact that the electronic continuum generated by A and B excitons depends on the excitation wavelength, and hence, the extent to which this continuum interacts with the discrete phonon also gets affected. A stronger Fano interaction (measured through a smaller q value) for a higher excitation wavelength is a clear signature of the presence of Fano resonance in the system.

Overall, the observed asymmetric Raman line shapes and their dependence on the excitation laser wavelength are due to the exciton quasi-continuum and phonon interaction as quantified using the Fano asymmetry parameter. The asymmetry in Raman line shape for the E^1_{2g} mode is toward the lower-wavenumber side (higher half width is less than the lower half width) along with the negative q value, representing a destructive interference between the electron continuum and discrete phonon mode. On the other hand, the asymmetry toward the higher-wavenumber side (higher half width is more than the lower half width) and a positive value or Fano parameter q obtained for the A_{1g} mode correspond to the constructive coupling of the electronic continuum with the discrete phonon.[60]

CONCLUSIONS

An asymmetric Raman line shape has been observed from MLMNs due to Fano interaction. Both the characteristic Raman modes of MLMNs, E^1_{2g} and A_{1g}, exhibit asymmetric spectral line shape and show good fit with the theoretical Fano−Raman line-shape function giving the first indication of possible Fano interaction. The presence of Fano interaction has been validated using wavelength-dependent variation in the Raman line shape which shows stronger Fano coupling for longer wavelengths, a typical observation from any system that possesses Fano interaction. The asymmetric Raman line shape obtained using 633 nm laser excitation is compared with the 532 nm one, and a smaller value of q, the Fano parameter that quantifies the coupling strength, was obtained for 633 nm excitation than for 532 nm, which validates the typical wavelength dependence of Fano interaction. The interaction is likely taking place between the quasi-continuum present by means of A and B excitons and the discrete vibronic levels. Varying electronic continuum due to different laser excitations appears to be the most likely reason for such wavelength-dependent electron−phonon interaction. Raman line shape analysis, carried out at two different wavelengths, proves to be helpful in gaining an understanding of electron−phonon interaction in 2D materials which may help in better device design and in understanding carrier dynamics. A similar study could be extended for various 2D materials like MoS_2 monolayers, WS_2, etc. to understand the phonon mechanism in 2D materials.

AUTHOR INFORMATION

Corresponding Author

Rajesh Kumar − *Materials and Device Laboratory, Department of Physics, Indian Institute of Technology Indore, Indore 453552, India; Centre for Indian Scientific Knowledge Systems and Centre for Advanced Electronics, Indian Institute of Technology Indore, Indore 453552, India;* orcid.org/0000-0001-7977-986X; Email: rajeshkumar@iiti.ac.in

Authors

Manushree Tanwar − *Materials and Device Laboratory, Department of Physics, Indian Institute of Technology Indore, Indore 453552, India;* orcid.org/0000-0002-7589-0496

Love Bansal − *Materials and Device Laboratory, Department of Physics, Indian Institute of Technology Indore, Indore 453552, India*

https://doi.org/10.1021/acsphyschemau.2c00021
ACS Phys. Chem Au 2022, 2, 417−422

Chanchal Rani − *Materials and Device Laboratory, Department of Physics, Indian Institute of Technology Indore, Indore 453552, India*
Sonam Rani − *Department of Physics, Guru Jambheshwar University of Science & Technology, Hisar 125001, India*
Suchita Kandpal − *Materials and Device Laboratory, Department of Physics, Indian Institute of Technology Indore, Indore 453552, India*
Tanushree Ghosh − *Materials and Device Laboratory, Department of Physics, Indian Institute of Technology Indore, Indore 453552, India;* orcid.org/0000-0001-7160-685X
Devesh K. Pathak − *Materials and Device Laboratory, Department of Physics, Indian Institute of Technology Indore, Indore 453552, India;* orcid.org/0000-0002-2367-787X
I. Sameera − *Department of Physics, Guru Jambheshwar University of Science & Technology, Hisar 125001, India;* orcid.org/0000-0002-6689-1075
Ravi Bhatia − *Department of Physics, Guru Jambheshwar University of Science & Technology, Hisar 125001, India*

Complete contact information is available at: https://pubs.acs.org/10.1021/acsphyschemau.2c00021

Notes

The authors declare no competing financial interest.

■ ACKNOWLEDGMENTS

Authors acknowledge financial support from the Science and Engineering Research Board, Govt. of India (Grant no. CRG/2019/000371). Authors are thankful to Er. Nitin Upadhyay for technical support. One of the authors (L.B.) acknowledges the Council of Scientific and Industrial Research (CSIR) for financial assistance [file no. 09/1022(12309)/2021-EMR-I]. Authors T.G. and M.T. acknowledge IIT Indore and the Department of Science and Technology (DST), (file DST/INSPIRE/03/2018/000910/IF180398), Government of India, for providing fellowships. Author C.R. acknowledges the DST (DST/INSPIRE/03/2019/002160/IF190314), and author S.K. acknowledges the UGC (Ref. 1304-JUNE-2018-513215), Govt. of India, for providing fellowships. Facilities received from the DST, Govt. of India, under the FIST scheme (grant number S.R./FST/PSI-225/2016) are highly acknowledged. S. Rani is thankful to DST, New Delhi for the financial aid. I. Sameera & R. Bhatia are thankful to DST, New Delhi (India) for the research grant in the form of Inspire Faculty Awards [DST/INSPIRE04/2017/002776 & DST/INSPIRE/04/2015/000902]. We thank Department of Science and Technology, New Delhi for providing XRD facilities (FIST scheme SR/FST/PSI-089/2005).

■ ABBREVIATIONS

FET	field-effect transistor
fwhm	full width at half-maximum
MLMNs	multi-layered MoS_2 nanoflakes

■ REFERENCES

(1) Wurstbauer, U.; Miller, B.; Parzinger, E.; Holleitner, A. W. Light−Matter Interaction in Transition Metal Dichalcogenides and Their Heterostructures. *J. Phys. D: Appl. Phys.* **2017**, *50*, 173001.
(2) Kandpal, S.; Ghosh, T.; Rani, C.; Rani, S.; Pathak, D. K.; Tanwar, M.; Bhatia, R.; Sameera, I.; Kumar, R. MoS_2 Nano-Flower Incorporation for Improving Organic-Organic Solid State Electrochromic Device Performance. *Sol. Energy Mater. Sol. Cells* **2021**, *236*, 111502.
(3) Mak, K. F.; Lee, C.; Hone, J.; Shan, J.; Heinz, T. F. Atomically Thin **MoS_2**: A New Direct-Gap Semiconductor. *Phys. Rev. Lett.* **2010**, *105*, 136805.
(4) Kandpal, S.; Ghosh, T.; Rani, C.; Tanwar, M.; Sharma, M.; Rani, S.; Pathak, D. K.; Bhatia, R.; Sameera, I.; Jayabalan, J.; Kumar, R. Bifunctional Application of Viologen-MoS_2-CNT/Polythiophene Device as Electrochromic Diode and Half-Wave Rectifier. *ACS Mater. Au* **2022**, *2*, 293 DOI: 10.1021/acsmaterialsau.1c00064.
(5) Choudhury, P.; Ravavarapu, L.; Dekle, R.; Chowdhury, S. Modulating Electronic and Optical Properties of Monolayer MoS_2 Using Nonbonded Phthalocyanine Molecules. *J. Phys. Chem. C* **2017**, *121*, 2959−2967.
(6) Yin, X.; Ye, Z.; Chenet, D. A.; Ye, Y.; O'Brien, K.; Hone, J. C.; Zhang, X. Edge Nonlinear Optics on a MoS_2 Atomic Monolayer. *Science* **2014**, *344*, 488−490.
(7) Kim, I. S.; Sangwan, V. K.; Jariwala, D.; Wood, J. D.; Park, S.; Chen, K.-S.; Shi, F.; Ruiz-Zepeda, F.; Ponce, A.; Jose-Yacaman, M.; Dravid, V. P.; Marks, T. J.; Hersam, M. C.; Lauhon, L. J. Influence of Stoichiometry on the Optical and Electrical Properties of Chemical Vapor Deposition Derived MoS_2. *ACS Nano* **2014**, *8*, 10551−10558.
(8) Lopez-Sanchez, O.; Lembke, D.; Kayci, M.; Radenovic, A.; Kis, A. Ultrasensitive Photodetectors Based on Monolayer MoS_2. *Nat. Nanotechnol.* **2013**, *8*, 497−501.
(9) Butun, S.; Tongay, S.; Aydin, K. Enhanced Light Emission from Large-Area Monolayer MoS_2 Using Plasmonic Nanodisc Arrays. *Nano Lett.* **2015**, *15*, 2700−2704.
(10) Guan, Z.; Lian, C.-S.; Hu, S.; Ni, S.; Li, J.; Duan, W. Tunable Structural, Electronic, and Optical Properties of Layered Two-Dimensional C2N and MoS_2 van Der Waals Heterostructure as Photovoltaic Material. *J. Phys. Chem. C* **2017**, *121*, 3654−3660.
(11) Zhang, J.; Zhu, Y.; Tebyetekerwa, M.; Li, D.; Liu, D.; Lei, W.; Wang, L.; Zhang, Y.; Lu, Y. Vanadium-Doped Monolayer MoS_2 with Tunable Optical Properties for Field-Effect Transistors. *ACS Appl. Nano Mater.* **2021**, *4*, 769−777.
(12) Ganatra, R.; Zhang, Q. Few-Layer MoS_2: A Promising Layered Semiconductor. *ACS Nano* **2014**, *8*, 4074−4099.
(13) Butler, W. H.; Williams, R. K. Electron-Phonon Interaction and Lattice Thermal Conductivity. *Phys. Rev. B: Solid State* **1978**, *18*, 6483−6494.
(14) Rai, D. P.; Vu, T. V.; Laref, A.; Hossain, M. A.; Haque, E.; Ahmad, S.; Khenata, R.; Thapa, R. K. Electronic Properties and Low Lattice Thermal Conductivity (Kl) of Mono-Layer (ML) MoS_2: FP-LAPW Incorporated with Spin−Orbit Coupling (SOC). *RSC Adv.* **2020**, *10*, 18830−18840.
(15) Nie, Z.; Shi, Y.; Qin, S.; Wang, Y.; Jiang, H.; Zheng, Q.; Cui, Y.; Meng, Y.; Song, F.; Wang, X.; Turcu, I. C. E.; Wang, X.; Xu, Y.; Shi, Y.; Zhao, J.; Zhang, R.; Wang, F. Tailoring Exciton Dynamics of Monolayer Transition Metal Dichalcogenides by Interfacial Electron-Phonon Coupling. *Commun. Phys.* **2019**, *2*, 103.
(16) Fano, U. Effects of Configuration Interaction on Intensities and Phase Shifts. *Phys. Rev.* **1961**, *124*, 1866−1878.
(17) Kroner, M.; Govorov, A. O.; Remi, S.; Biedermann, B.; Seidl, S.; Badolato, A.; Petroff, P. M.; Zhang, W.; Barbour, R.; Gerardot, B. D.; Warburton, R. J.; Karrai, K. The Nonlinear Fano Effect. *Nature* **2008**, *451*, 311−314.
(18) Yogi, P.; Mishra, S.; Saxena, S. K.; Kumar, V.; Kumar, R. Fano Scattering: Manifestation of Acoustic Phonons at the Nanoscale. *J. Phys. Chem. Lett.* **2016**, *7*, 5291−5296.
(19) Raman, C. A. New Radiation. *Indian J. Phys.* **1928**, *02*, 387−398.
(20) Raman, C. V.; Krishnan, K. S. A New Type of Secondary Radiation. *Nature* **1928**, *121*, 501−502.
(21) Tanwar, M.; Saxena, S. K.; Kumar, R. Raman Spectromicroscopy: A Tool to "See" Subtle Aspects in Science, Technology, and Engineering. *J. Phys. Chem. C* **2022**, *126*, 4733−4743.
(22) Kumar, R.; Tanwar, M. Effect of Some Physical Perturbations and Their Interplay on Raman Spectral Line Shapes in Silicon: A Brief Review. *J. Raman Spectrosc.* **2021**, *52*, 2100−2118.

(23) Rani, C.; Tanwar, M.; Ghosh, T.; Kandpal, S.; Pathak, D. K.; Chaudhary, A.; Yogi, P.; Saxena, S. K.; Kumar, R. Raman Spectroscopy as a Simple yet Effective Analytical Tool for Determining Fermi Energy and Temperature Dependent Fermi Shift in Silicon. *Anal. Chem.* **2022**, *94*, 1510−1514.
(24) Chaudhary, A.; Pathak, D. K.; Tanwar, M.; Kumar, R. Tracking Dynamic Doping in a Solid-State Electrochromic Device: Raman Microscopy Validates the Switching Mechanism. *Anal. Chem.* **2020**, *92*, 6088−6093.
(25) Burke, B. G.; Chan, J.; Williams, K. A.; Wu, Z.; Puretzky, A. A.; Geohegan, D. B. Raman Study of Fano Interference in P-Type Doped Silicon. *J. Raman Spectrosc.* **2010**, *41*, 1759−1764.
(26) Tanwar, M.; Pathak, D. K.; Rani, C.; Kandpal, S.; Ghosh, T.; Mondal, P.; Chaudhary, A.; Kumar, R. Inverse Size Dependent Fano Parameter in Silicon Porous Wires: Consequence of Quasi-Continuum Flattening. *J. Phys. Chem. C* **2021**, *125*, 12767−12773.
(27) Kumar, R.; Mavi, H. S.; Shukla, A. K.; Vankar, V. D. Photoexcited Fano Interaction in Laser-Etched Silicon Nanostructures. *J. Appl. Phys.* **2007**, *101*, 064315.
(28) Magidson, V.; Beserman, R. Fano-Type Interference in the Raman Spectrum of Photoexcited Si. *Phys. Rev. B: Solid State* **2002**, *66*, 195206.
(29) Miroshnichenko, A. E.; Flach, S.; Kivshar, Y. S. Fano Resonances in Nanoscale Structures. *Rev. Mod. Phys.* **2010**, *82*, 2257−2298.
(30) Tanwar, M.; Pathak, D. K.; Chaudhary, A.; Krylov, A. S.; Pfnür, H.; Sharma, A.; Ahn, B.; Lee, S.; Kumar, R. Pseudo-Anomalous Size-Dependent Electron−Phonon Interaction in Graded Energy Band: Solving the Fano Paradox. *J. Phys. Chem. Lett.* **2021**, *12*, 2044−2051.
(31) Tanwar, M.; Pathak, D. K.; Chaudhary, A.; Yogi, P.; Saxena, S. K.; Kumar, R. Mapping Longitudinal Inhomogeneity in Nanostructures Using Cross-Sectional Spatial Raman Imaging. *J. Phys. Chem. C* **2020**, *124*, 6467−6471.
(32) Yogi, P.; Poonia, D.; Mishra, S.; Saxena, S. K.; Roy, S.; Kumar, V.; Sagdeo, P. R.; Kumar, R. Spectral Anomaly in Raman Scattering from P-Type Silicon Nanowires. *J. Phys. Chem. C* **2017**, *121*, 5372−5378.
(33) Chakraborty, B.; Matte, H. S. S. R.; Sood, A. K.; Rao, C. N. R. Layer-Dependent Resonant Raman Scattering of a Few Layer MoS_2. *J. Raman Spectrosc.* **2013**, *44*, 92−96.
(34) Molina-Sánchez, A.; Wirtz, L. Phonons in Single-Layer and Few-Layer MoS${}_{2}$ and WS${}_{2}$. *Phys. Rev. B: Condens. Matter Mater. Phys.* **2011**, *84*, 155413.
(35) Dhakal, K. P.; Duong, D. L.; Lee, J.; Nam, H.; Kim, M.; Kan, M.; Lee, Y. H.; Kim, J. Confocal Absorption Spectral Imaging of MoS_2: Optical Transitions Depending on the Atomic Thickness of Intrinsic and Chemically Doped MoS_2. *Nanoscale* **2014**, *6*, 13028−13035.
(36) Saigal, N.; Sugunakar, V.; Ghosh, S. Exciton Binding Energy in Bulk MoS_2: A Reassessment. *Appl. Phys. Lett.* **2016**, *108*, 132105.
(37) Mishra, S.; Lambora, S.; Yogi, P.; Sagdeo, P. R.; Kumar, R. Organic Nanostructures on Inorganic Ones: An Efficient Electrochromic Display by Design. *ACS Appl. Nano Mater.* **2018**, *1*, 3715−3723.
(38) Chaudhary, A.; Pathak, D. K.; Tanwar, M.; Koch, J.; Pfnür, H.; Kumar, R.; Kumar, R. Polythiophene-NanoWO 3 Bilayer as an Electrochromic Infrared Filter: A Transparent Heat Shield. *J. Mater. Chem. C* **2020**, *8*, 1773−1780.
(39) Pathak, D. K.; Chaudhary, A.; Tanwar, M.; Goutam, U. K.; Mondal, P.; Kumar, R. Nickel Cobalt Oxide Nanoneedles for Electrochromic Glucose Sensors. *ACS Appl. Nano Mater.* **2021**, *4*, 2143−2152.
(40) Pathak, D. K.; Chaudhary, A.; Tanwar, M.; Goutam, U. K.; Pfnür, H.; Kumar, R. Chronopotentiometric Deposition of Nano-cobalt Oxide for Electrochromic Auxiliary Active Electrode Application. *Phys. Status Solidi* **2020**, *217*, 2000173.
(41) Choudhary, N.; Park, J.; Hwang, J. Y.; Choi, W. Growth of Large-Scale and Thickness-Modulated MoS_2 Nanosheets. *ACS Appl. Mater. Interfaces* **2014**, *6*, 21215−21222.
(42) Yogi, P.; Saxena, S. K.; Mishra, S.; Rai, H. M.; Late, R.; Kumar, V.; Joshi, B.; Sagdeo, P. R.; Kumar, R. Interplay between Phonon Confinement and Fano Effect on Raman Line Shape for Semiconductor Nanostructures: Analytical Study. *Solid State Commun.* **2016**, *230*, 25−29.
(43) Saxena, S. K.; Borah, R.; Kumar, V.; Rai, H. M.; Late, R.; Sathe, V. G.; Kumar, A.; Sagdeo, P. R.; Kumar, R. Raman Spectroscopy for Study of Interplay between Phonon Confinement and Fano Effect in Silicon Nanowires. *J. Raman Spectrosc.* **2016**, *47*, 283−288.
(44) Sharma, M.; Rani, S.; Pathak, D. K.; Bhatia, R.; Kumar, R.; Sameera, I. Manifestation of Anharmonicities in Terms of Phonon Modes' Energy and Lifetime in Multiwall Carbon Nanotubes. *Carbon* **2021**, *171*, 568−574.
(45) Sharma, M.; Rani, S.; Pathak, D. K.; Bhatia, R.; Kumar, R.; Sameera, I. Temperature Dependent Raman Modes of Reduced Graphene Oxide: Effect of Anharmonicity, Crystallite Size and Defects. *Carbon* **2021**, *184*, 437−444.
(46) Pawbake, A. S.; Pawar, M. S.; Jadkar, S. R.; Late, D. J. Large Area Chemical Vapor Deposition of Monolayer Transition Metal Dichalcogenides and Their Temperature Dependent Raman Spectroscopy Studies. *Nanoscale* **2016**, *8*, 3008−3018.
(47) Neeshu, K.; Rani, C.; Kaushik, R.; Tanwar, M.; Pathak, D.; Chaudhary, A.; Kumar, A.; Kumar, R. Size Dependence of Raman Line-Shape Parameters Due to Confined Phonons in Silicon Nanowires. *Adv. Mater. Process Technol.* **2020**, *6*, 669−676.
(48) Kaushik, R.; Rani, C.; Neeshu, K.; Tanwar, M.; Pathak, D. K.; Chaudhary, A.; Siraj, F.; Jha, H. C.; Kumar, R. Brain Tumour Detection and Grading Using Raman Scattering: Analogy from Semiconductors for Solving Biological Problem. *Advances in Materials and Processing Technologies* **2020**, *0*, 1−12.
(49) Najafi, L.; Bellani, S.; Martín-García, B.; Oropesa-Nuñez, R.; Del Rio Castillo, A. E.; Prato, M.; Moreels, I.; Bonaccorso, F. Solution-Processed Hybrid Graphene Flake/2H-MoS_2 Quantum Dot Heterostructures for Efficient Electrochemical Hydrogen Evolution. *Chem. Mater.* **2017**, *29*, 5782−5786.
(50) Li, H.; Zhang, Q.; Yap, C. C. R.; Tay, B. K.; Edwin, T. H. T.; Olivier, A.; Baillargeat, D. From Bulk to Monolayer MoS_2: Evolution of Raman Scattering. *Adv. Funct. Mater.* **2012**, *22*, 1385−1390.
(51) Zhan, Y.; Liu, Z.; Najmaei, S.; Ajayan, P. M.; Lou, J. Large-Area Vapor-Phase Growth and Characterization of MoS_2 Atomic Layers on a SiO2 Substrate. *Small* **2012**, *8*, 966−971.
(52) Hasdeo, E. H.; Nugraha, A. R. T.; Dresselhaus, M. S.; Saito, R. Breit-Wigner-Fano Line Shapes in Raman Spectra of Graphene. *Phys. Rev. B: Condens. Matter Mater. Phys.* **2014**, *90*, 245140.
(53) Zhang, W.; Govorov, A. O.; Bryant, G. W. Semiconductor-Metal Nanoparticle Molecules: Hybrid Excitons and the Nonlinear Fano Effect. *Phys. Rev. Lett.* **2006**, *97*, 146804.
(54) Lee, C.; Yan, H.; Brus, L. E.; Heinz, T. F.; Hone, J.; Ryu, S. Anomalous Lattice Vibrations of Single- and Few-Layer MoS_2. *ACS Nano* **2010**, *4*, 2695−2700.
(55) Cerdeira, F.; Fjeldly, T. A.; Cardona, M. Interaction between Electronic and Vibronic Raman Scattering in Heavily Doped Silicon. *Solid State Commun.* **1973**, *13*, 325−328.
(56) Cerdeira, F.; Fjeldly, T. A.; Cardona, M. Effect of Free Carriers on Zone-Center Vibrational Modes in Heavily Doped p-Type Si. II. Optical Modes. *Phys. Rev. B: Solid State* **1973**, *8*, 4734−4745.
(57) Mueller, T.; Malic, E. Exciton Physics and Device Application of Two-Dimensional Transition Metal Dichalcogenide Semiconductors. *npj 2D Mater. Appl.* **2018**, *2*, 1−12.
(58) Kumar, R. Asymmetry to Symmetry Transition of Fano Line-Shape: Analytical Description. *Indian J. Phys.* **2013**, *87*, 49−52.
(59) Cerdeira, F.; Fjeldly, T. A.; Cardona, M. Raman Study of the Interaction between Localized Vibrations and Electronic Excitations in Boron-Doped Silicon. *Phys. Rev. B: Solid State* **1974**, *9*, 4344−4350.
(60) Sunny, A.; Thirumurugan, A.; Balasubramanian, K. Laser Induced Fano Scattering, Electron−Phonon Coupling, Bond Length and Phonon Lifetime Changes in α-Fe2O3 Nanostructures. *Phys. Chem. Chem. Phys.* **2020**, *22*, 2001−2009.

https://doi.org/10.1021/acsphyschemau.2c00021
ACS Phys. Chem Au 2022, 2, 417−422